BULLETIN DE L'ASSOCIATION MINERALOGIQUE DU CANADA

THE CANADIAN MINERALOGIST

JOURNAL OF THE MINERALOGICAL ASSOCIATION OF CANADA

Volume 28 June 1990 Part 2

Canadian Mineralogist
Vol. 28, pp. 189-206 (1990)

PETROLOGY OF Au–Ag–Hg ALLOY AND "INVISIBLE" GOLD IN THE TROUT LAKE MASSIVE SULFIDE DEPOSIT, FLIN FLON, MANITOBA

RAYMOND E. HEALY

Department of Geological Sciences, University of Manitoba, Winnipeg, Manitoba R3T 2N2

WILLIAM PETRUK

Mineral Processing Laboratory, CANMET, 555 Booth Street, Ottawa, Ontario K1A 0G1

ABSTRACT

Gold in the volcanogenic massive sulfide ores at Trout Lake, Flin Flon, Manitoba occurs mainly as a Au–Ag–Hg alloy, but is also present in minor amounts as "invisible" gold in pyrite and arsenopyrite. Two textural types of the alloy are defined: (1) inclusions, interstitial material and fracture fillings in, and coatings on, pyrite grains, and (2) anastomosing masses ($\leq$5 mm) along the folded contact between laminae of massive chalcopyrite and chlorite schist. The median grain-size of the Au–Ag–Hg alloy is 11 μm, with 75% finer than 21 μm. The average composition (wt.%) of the mineral is 49.2% Ag, 38.7% Au and 11.0% Hg, and the ranges are 17.3 to 76.5% Ag, 1.62 to 79.9% Au, and 1.29 to 30.9% Hg. The compositional variation reflects extensive solid-solution within the extrapolated stability field for the α-phase in the system Ag–Au–Hg. High-contrast back-scattered electron photographs reveal systematic zoning, and a general sequence of crystallization of increasingly Ag-rich compositions. This sequence reflects the increased activity of bisulfide complexes of Ag compared to those of Au and Hg in the evolved pore-fluids during retrograde metamorphism, and its episodic diffusion into earlier formed, more intermediate compositions, under disequilibrium conditions. The average "invisible" gold content, determined by SIMS analysis, is 0.72 ppm in arsenic-poor pyrite, and 30.2 ppm in arsenopyrite. Approximately 93% of the Au in the ore occurs as Au–Ag–Hg alloy, with 6 and 1% as "invisible" gold in pyrite and arsenopyrite, respectively.

Keywords: Au–Ag–Hg alloy, α-phase, mineral chemistry, gold, "invisible" gold, hydrothermal transport, bisulfide complexes, volcanogenic massive sulfides, Trout Lake, Flin Flon, Manitoba.

SOMMAIRE

L'or qui se trouve dans les sulfures massifs volcanogéniques du gisement de Trout Lake, à Flin Flon, au Manitoba, y figure surtout sous forme d'alliage de Au–Ag–Hg, et aussi, en quantités inférieures, sous forme d'or dit "invisible" dans la pyrite et l'arsenopyrite. L'alliage présente deux textures: 1) en inclusions, dans les interstices et les fissures et comme surcroissances sur les grains de pyrite, et 2) en masses ($\leq$5 mm) qui s'enchevêtrent le long du contact ondulant entre des lisières de chalcopyrite massive et un schiste chloriteux. Les grains de cet alliage ont une taille moyenne de 11 μm, et 75% des grains ne dépassent pas 21 μm. L'alliage contient, en moyenne, 49.2% Ag (en poids), 38.7% Au et 11.0% Hg; les proportions pondérales tombent dans les intervalles suivants: 17.3–76.5% Ag, 1.62–79.9% Au, et 1.29–30.9% Hg. La variation en composition exprime l'existence d'une solution solide étendue dans le champ de stabilité de la phase α, défini par extrapolation dans le système Ag–Au–Hg. Des photographies à contraste élevé des électrons rétrodiffusés révèlent une zonation systématique et une séquence de cristallisation vers des compositions progressivement plus riches en Ag. Cette séquence résulterait de l'activité accrue des complexes bisulfurés d'Ag plutôt que ceux d'Au ou de Hg dans les fluides interstitiels évolués qui circulaient lors du métamorphisme rétrograde, et de leur diffusion épisodique sous conditions de déséquilibre dans des compositions plus intermédiaires formées antérieurement. La teneur moyenne en or "invi-

sible", telle que déterminée par analyse SIMS, serait 0.72 ppm dans la pyrite à faible teneur en As, et 30.2 ppm dans l'arsenopyrite. Environ 93% de l'or dans le minerai apparaît sous forme d'alliage, et 6% et 1% sous forme d'or "invisible" dans la pyrite et l'arsenopyrite, respectivement.

(Traduit par la Rédaction)

Mots-clés: alliage de Au–Ag–Hg, phase α, chimie minérale, or, or "invisible", transfert hydrothermal, complexes bisulfurés, sulfures massifs volcanogéniques, gisement de Trout Lake, Flin Flon, Manitoba.

Introduction

Mineralogical studies of the ores from the Trout Lake massive sulfide deposit (Healy & Petruk 1988), and of the mill products from the Trout Lake concentrator circuit (Healy & Petruk 1989), were undertaken to determine the mineralogical characteristics that affect metal recoveries from the ores. Previously, the host of the Au had not been identified with confidence, the sole published reference being to a "metallic gold" mineral (Muzylowski 1979). During the current mineralogical study of the ores and mill products, an abundant Au–Ag–Hg alloy was identified, and "invisible" gold was detected in pyrite and arsenopyrite. In this paper, we describe the occurrence and mineralogical character of the Au–Ag–Hg alloy, and present results of analyses for "invisible" gold.

Geological Setting

The Trout Lake deposit is located 5 km northeast of Flin Flon, Manitoba, in the Amisk Group of volcanic strata in the Proterozoic Flin Flon greenstone belt. The Flin Flon belt forms part of the southern Churchill structural province; in the vicinity of the Trout Lake deposit, it was deformed and metamorphosed to the middle greenschist facies prior to 1,750 Ma during the Hudsonian Orogeny (Syme *et al.* 1982). The Amisk Group comprises the lower stratigraphic elements of the Flin Flon belt, and is dominated by subaqueous and subaerial volcanic rocks deposited in an Aphebian island-arc setting. The volcanic rocks consist of massive to pillowed basalt and andesite flows, overlain by pyroclastic andesitic breccias, and rhyolitic and dacitic quartz porphyries (Koo & Mossman 1975).

Ore Deposit

The Trout Lake deposit, which grades 3.8% Zn, 2.4% Cu, 0.04% Pb, 15.9 ppm Ag and 1.7 ppm Au (Ko 1986), is a metamorphosed volcanogenic massive sulfide deposit, as defined by Franklin *et al.* (1981). It consists of a series of steeply dipping stacked lenses (6 proven) occurring in two zones that strike 140° and have a relatively constant dip of 60–70° to the northeast (Ko 1986). Each lens comprises two principal types of mineralization: massive sulfides occur in quartz–sericite schists, and semimassive to disseminated sulfides occur in the footwall chlorite schists. The host rocks represent the metamorphosed equivalents of hydrothermally altered fragmental pyroclastic quartz porphyry. The massive sulfides represent exhalative mineralization deposited on the seafloor proximal to a fumarolic vent. The semimassive to disseminated mineralization is interpreted as the tectonically flattened equivalent of the stockwork mineralization (C. Ko, pers. comm. 1985).

The ores were classified into nine types (Table 1) on the bases of quantities and textures of the ore minerals (Healy & Petruk 1988). The mineralogy of the ores is presented in a generalized upward strati-

TABLE 1. MINERALOGICAL COMPOSITION OF THE ORE TYPES*

	Massive Sphal.	Layered Py+Sphal.	Massive Py.	Layered Cpy+Sphal.	Massive Cpy+Po.	Cpy Stringers.	Dissem. Py+Cpy.	Sheared Cpy+Sphal.	Vein Qtz+Cpy.
Gangue	20.16	18.11	18.42	30.28	20.91	32.96	61.54	31.52	86.84
Pyrite**	5.15	42.44	74.85	16.30	21.31	20.35	38.46	3.33	2.14
Pyrrhotite	2.70	0.02	0.01	7.70	21.30	5.00	0.03	11.00	0.90
Sphalerite	63.20	33.17	5.57	29.60	0.70	4.60	0.58	38.70	0.72
Chalcopyrite***	5.10	1.77	0.56	16.00	35.70	36.50	3.90	15.40	9.40
Galena	3.60	1.25	0.34	0.01	0.00	0.05	0.01	0.01	0.00
Arsenopyrite	0.09	3.24	0.25	0.08	0.07	0.54	0.05	0.04	0.00
Au-Ag-Hg Alloy****	0.00036	0.00098	0.00025	0.00097	0.00080	0.00054	0.00024	0.00165	0.00148

* Volume% determined by image analysis and calculations from assays; ** Includes minor marcasite and magnetite; *** Includes cubanite; **** Calculated from assays.
Other minerals observed in the ores are freibergite, gudmundite, pyrargyrite, dyscrasite, boulangerite, freieslebenite, costibite, clausthalite, hessite, rucklidgeite and pilsenite (Healy & Petruk 1988), and bournonite, volynskite, naumannite and acanthite in the mill products (Healy & Petruk 1989).

graphic order (left to right in Table 1) except for Sheared Chalcopyrite + Sphalerite, and Vein Quartz + Chalcopyrite ore types. These latter two were produced by tectonic processes and exhibit little stratigraphic control.

The lenses generally show a metal zonation; high Ag and Pb concentrations are associated with low Cu/(Cu + Zn) values in the hanging wall, whereas high Au concentrations are associated with high Cu/(Cu + Zn) values in the footwall. This zonation is characteristic of many volcanogenic massive sulfides (Large 1977, Franklin *et al.* 1981), and is widely accepted as having been generated by the evolving hydrothermal system according to the model of Eldridge *et al.* (1983). The general preservation of the primary Cu/(Cu + Zn) zonation suggests that large-scale redistribution of elements due to metamorphic remobilization has not occurred at Trout Lake.

Characteristics of the Au–Ag–Hg Alloy

A gold-bearing mineral whose optical properties are similar to those of electrum was observed in 37 of 112 samples. The mineral shows a wide range in composition: 17.3 to 76.5 wt.% Ag, 1.6 to 79.9% Au and 1.3 to 30.9% Hg. This compositional range constitutes an extension of the continuous binary Au–Ag solid solution into the ternary system Ag–Au–Hg. These ternary alloys have been referred to as gold-silver amalgam (Nysten 1986), mercurian electrum (Scott 1977, Healy & Petruk 1988, 1989), and mercurian gold (Shikazono & Shimizu 1988). However, none of these terms encompass the full range in compositions observed at Trout Lake. In this paper, the mineral will be referred to as a Au–Ag–Hg alloy, and encompasses the compositions of both mercurian gold and mercurian silver. This range of compositions should not be confused with that of other Au–Ag–Hg ternary alloys, *e.g.*, γ-goldamalgam (Dunn *et al.* 1985).

The Au–Ag–Hg alloy was found in all the ore types, except the Vein Quartz + Chalcopyrite ore type. The Au–Ag–Hg alloy is invariably a trace constituent, but in sample TLN.1–89 (Chalcopyrite Stringer ore), a 2-mm-long anastomosing mass com-

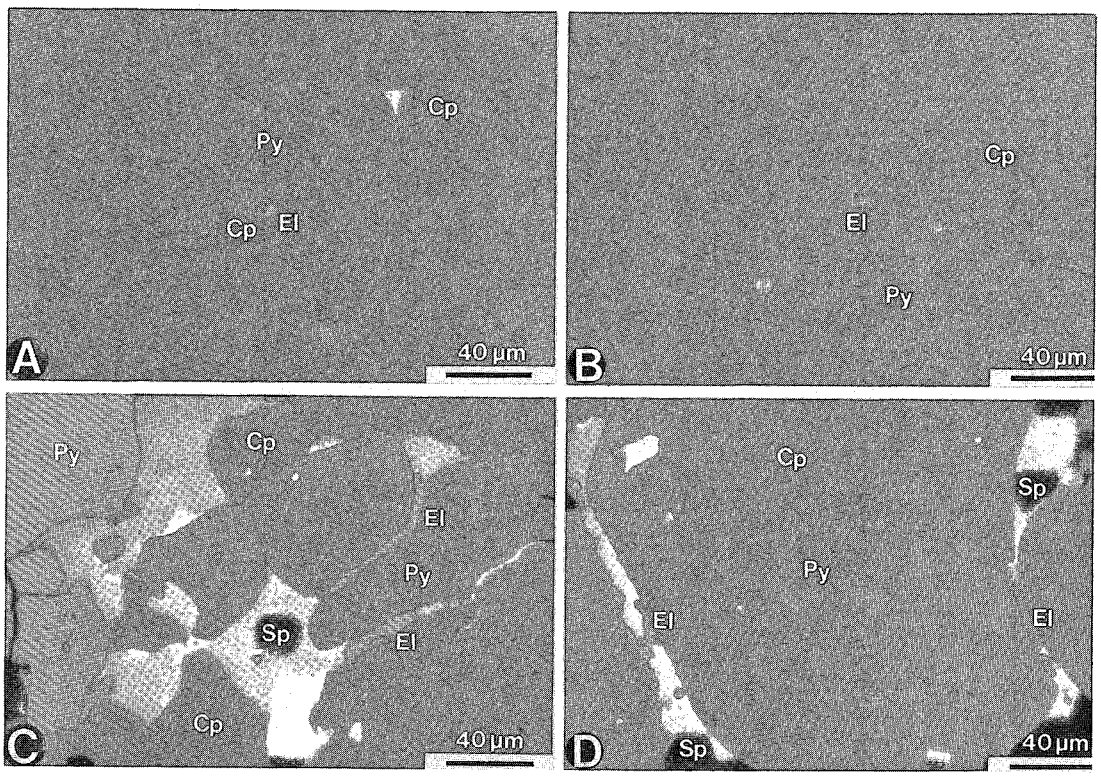

FIG. 1. Reflected-light photomicrographs of Type-1A Au–Ag–Hg alloy in TLN.2–8: (A) composite inclusion of alloy (El) and chalcopyrite (Cp) in pyrite (Py); (B) alloy inclusion on a fracture in pyrite; (C) alloy as a fracture filling in, and grain coating on pyrite, and associated with interstitial sphalerite and chalcopyrite; (D) alloy as grain coatings on pyrite and associated with interstitial sphalerite.

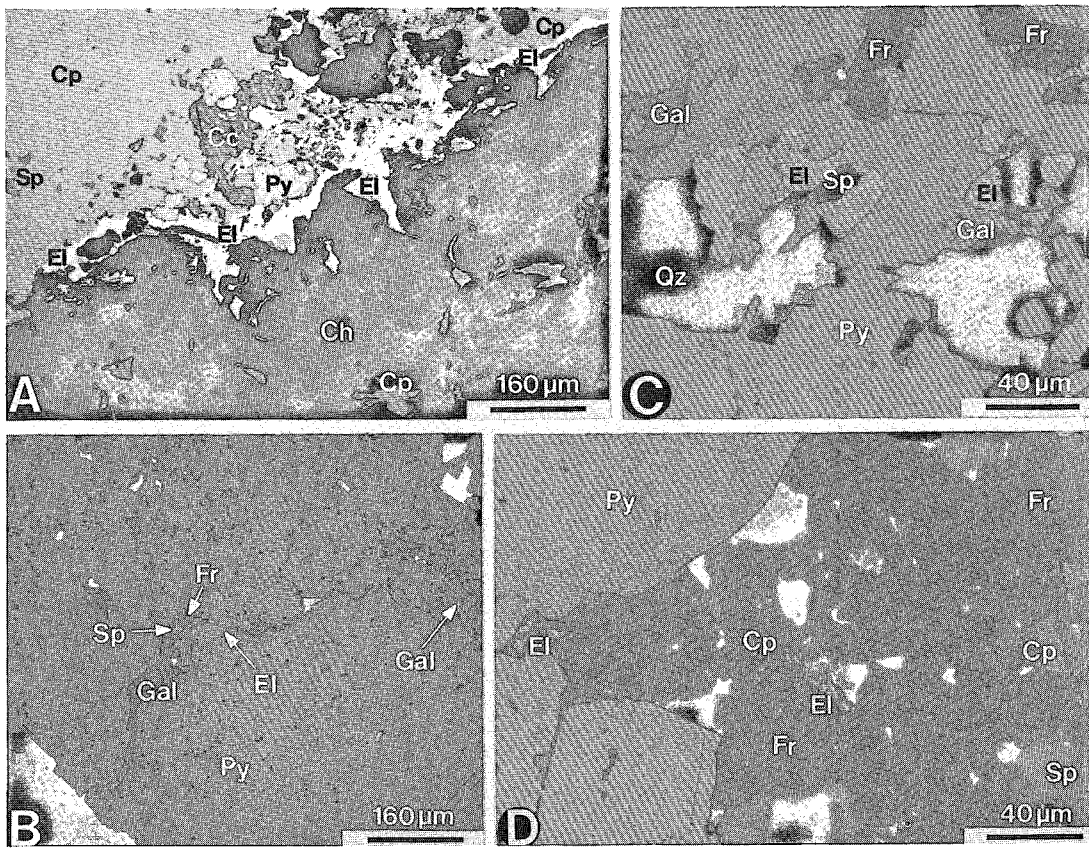

FIG. 2. Reflected-light photomicrographs of Au–Ag–Hg alloy: (A) TLN.1–89a: anastomosing mass of Type-2 alloy (El) along contact between chalcopyrite (Cp) and chlorite schist (Gan denotes silicate gangue) laminae (Cc denotes persistent carbon coat); (B) TLS.5–83: Type-1B alloy associated with galena (Gal), freibergite (Fr) and sphalerite (Sp) infilling a large fracture in pyrite (Py); (C) TLS.3–40: clusters of Type-1B alloy grains associated with freibergite, galena and quartz in pyrite; (D) TLS.3–40: fine-grained inclusions of Type-1B alloy in freibergite containing sphalerite and exsolved chalcopyrite.

prises 0.2 area % of the polished section. It occurs in the nose of a mesoscopic, disharmonic fold structure along the contact between laminae of massive chalcopyrite and chlorite schist. Additional sections coplanar to TLN.1-89(a) (*i.e.*, b to k) revealed similar masses on the same, and occasionally also on adjacent fold structures, over a distance of 9 cm.

The Au–Ag–Hg alloy occurs in two textural types. Type-1 Au–Ag–Hg alloy is texturally associated with pyrite and consists of: (A) fine-grained inclusions in pyrite (Fig. 1A), fracture fillings in pyrite (Figs. 1B, C), and grain coatings on the margins of, and as interstitial fillings between pyrite grains (Figs. 1C, D); and (B) grains encapsulated by and associated with galena, freibergite and minor arsenopyrite, which occur interstitially to, or as fracture fillings in, fractured pyrite (Figs. 2B, C, D). Type 1B was observed in 3 samples and is thus volumetrically insignificant; it is restricted to the Massive Pyrite and the Layered Pyrite + Sphalerite ore types. We distinguish Type 1B to emphasize that, although rare at Trout Lake, in our experiences the association of electrum or Au–Ag–Hg alloy with galena and freibergite is a distinctive assemblage in many Canadian massive sulfide deposits. Type-1 alloy is found in all but one ore type, and is by far the most common type. Approximately one third (*i.e.*, 103) of all Type-1A grains were found in a single polished section of TLN.2–8, a sample of Sheared Chalcopyrite + Sphalerite ore that occurs adjacent to a syntectonic quartz diorite sill.

Type-2 alloy was observed in TLN.1–89(a – k) and TLN.2–11 only, and consists of large (*i.e.*, <5 mm) anastomosing masses and lesser disseminations distributed along the contact between laminae of chalcopyrite and chlorite schist (Fig. 2A). Type 2 was

found only in the Chalcopyrite Stringer ores; in spite of its scarcity, it undoubtedly constitutes volumetrically the most significant type.

Grain sizes

The grain-size distribution of grains of Type-1 alloy was measured using a Reichert Zetoplan optical microscope with calibrated graticules. That of Type-2 alloy (sections TLN.2–11 and TLN.1–89a) was determined with the MP–SEM–IPS image analysis system at CANMET (Petruk 1987). The grain-size distributions for Types 1 and 2 are given in Figure 3. The two sections TLN.1–89a and TLN.2–11 contain approximately 600,000 μm^2 and 9,000 μm^2 of Type-2 alloy, respectively, whereas 417 grains of Type 1 in 35 samples cover approximately 11,000 μm^2. Despite this overwhelming predominance of Type 2, the relative abundance of Type 1 relative to Type 2 is not statistically constrained. Thus an unweighted average grain-size distribution for Trout Lake alloy was calculated by combining the data for Types 1 and 2; it is defined as 75% finer than 21 μm, with a median grain-size of 11 μm.

Chemical composition of the alloy

The mineral chemistry of Au–Ag–Hg alloy was investigated by electron-microprobe analysis (EMPA) using the JEOL 733 Superprobe, which forms an integral part of the MP–SEM–IPS system of image analysis (Petruk 1987). Concentrations of Ag, Au, Hg and Fe were determined by wavelength-dispersion analysis (WDA). Fe was sought because it had been observed consistently in energy-dispersion spectra on the MAC V electron microprobe at the University of Manitoba. High-contrast backscattered electron (BSE) imagery was used to select all analytical points. The counting scheme involved a collection time of 60 s or less (if acceptable counting statistics are achieved, *i.e.*, standard deviation = 0.5%) for all four elements on the standards and unknowns. Routine reduction of data, including full matrix (ZAF) corrections, was done. The principal operating parameters are given in Table 2. The detection limit for Au, Ag, Hg and Fe is 0.05 wt.%. Cu and S also were determined in twenty of the analyses. Furthermore, several profiles of Au, Ag and Hg concentrations by continuous qualitative wavelength-dispersion traverses across masses of Type-2 Au–Ag–Hg alloy were generated on the new CAMECA SX-50 electron microprobe at the University of Manitoba.

The wavelength-dispersion analyses of Au–Ag–Hg alloy show the consistent presence of Ag, Au and Hg in widely varying proportions, whereas Fe occurs in minor to undetectable amounts. The 104 analyses

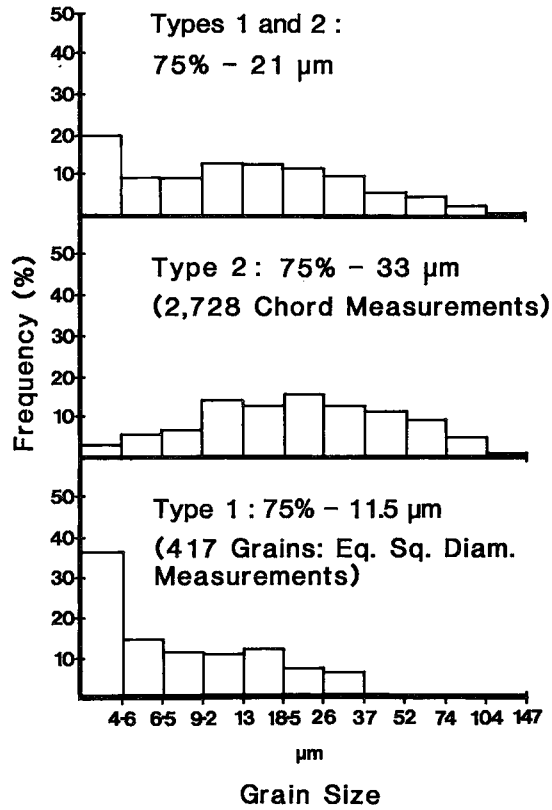

FIG. 3. Histograms of grain-size distributions in the Trout Lake Au–Ag–Hg alloy.

gave a mean composition (in wt.%) of 49.2% Ag, 38.7% Au, 11.0% Hg and 0.7% Fe. The ranges of elemental concentrations in the alloy are shown as histograms in Figure 4.

The Fe content is anomalous, as iron is not known to occur in native metals and alloys, as determined by microprobe analyses (L. Cabri, pers. comm. 1987). In contrast, Boyle (1979) suggested that Fe is probably a structural constituent of metallic gold. On the basis of the twenty analyses in which Cu and S also were determined, Healy & Petruk (in prep.) have concluded that the Fe is an analytical contaminant generated in an extensive volume of secondary fluorescence of Fe$K\alpha$ (fluoresced principally by Au$L\alpha$). We also conclude that microprobe analyses of minute grains (<20 μm in diameter) of gold, electrum and Au–Ag–Hg alloys encased in, or adjacent to, pyrite, chalcopyrite, arsenopyrite and pyrrhotite are apt to give contaminant-derived Fe values. Because only 28% of the Trout Lake Au–Ag–Hg alloy occurs as grains or masses greater than 20 μm in diameter, contaminant-free analyses are therefore largely unattainable. Thus the Fe detected seems not

TABLE 2. EIGHT REPRESENTATIVE COMPOSITIONS (MICROPROBE DATA) OF Au-Ag-Hg ALLOY FROM TROUT LAKE

Wt %	1 Ag-rich	2 Au-rich	3 Hg-rich	4 Hg-poor	5 Fe-rich	6 Typical	7 Typical	8 Typical	Average (n=104)	Uncertainty (95% Confidence)
Ag	76.47	17.34	66.28	27.85	47.59	43.03	48.51	49.87	49.22	±0.5 - 0.6
Au	11.17	79.86	1.62	67.18	35.24	43.96	38.75	30.55	38.68	±0.5 - 5.8
Hg	11.14	2.68	30.87	1.29	15.02	11.80	13.20	18.58	11.00	±0.5 - 3.8
Fe	nd.	0.55	1.59	2.20	2.74	0.30	nd.	0.39	0.70	±0.7 - nd.
Total	98.78	100.40	100.34	98.49	100.57	99.06	100.46	99.36	99.60	

nd. = not detected.
Analytical parameters:

Excitation voltage = 20 kV.
Sample current = 15 nA on the Faraday cup.
Ag : AgLα analytical line; PET crystal; Ag-Au alloy (71.6 wt % Ag, 28.4 wt % Au) standard.
Au : AuMα analytical line; PET crystal; Ag-Au alloy (50.1 wt % Ag, 49.9 wt % Au) standard.
Hg : HgLα analytical line; LIF crystal; synthetic Pd_3HgTe_3 standard.
Fe : FeKα analytical line; LIF crystal; Pyrite (FeS_2) standard.
Note : Fe content is contaminant-derived.

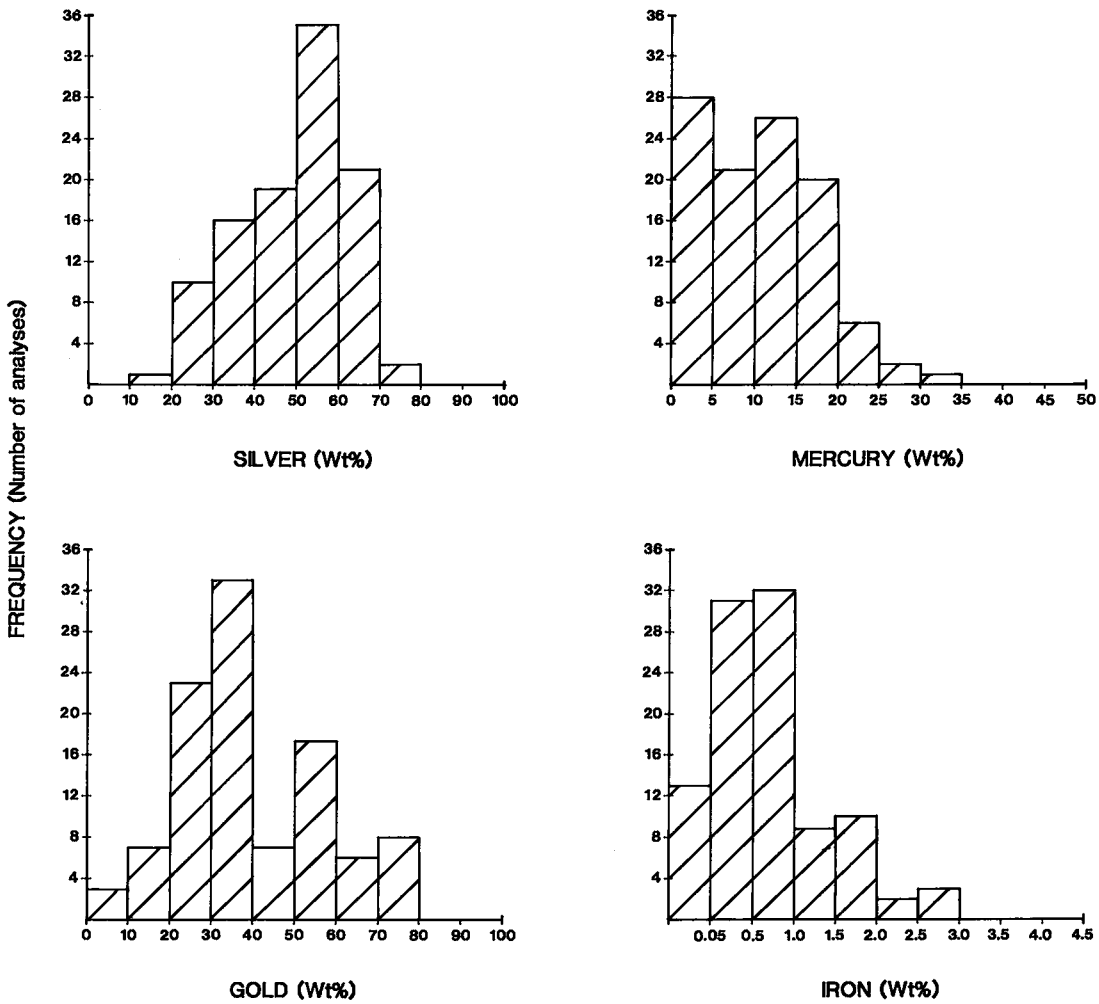

FIG. 4. Histograms displaying the range of Ag, Au, Hg and Fe compositions (microprobe data) in Trout Lake Au-Ag-Hg alloy. Fe is due to analytical contamination.

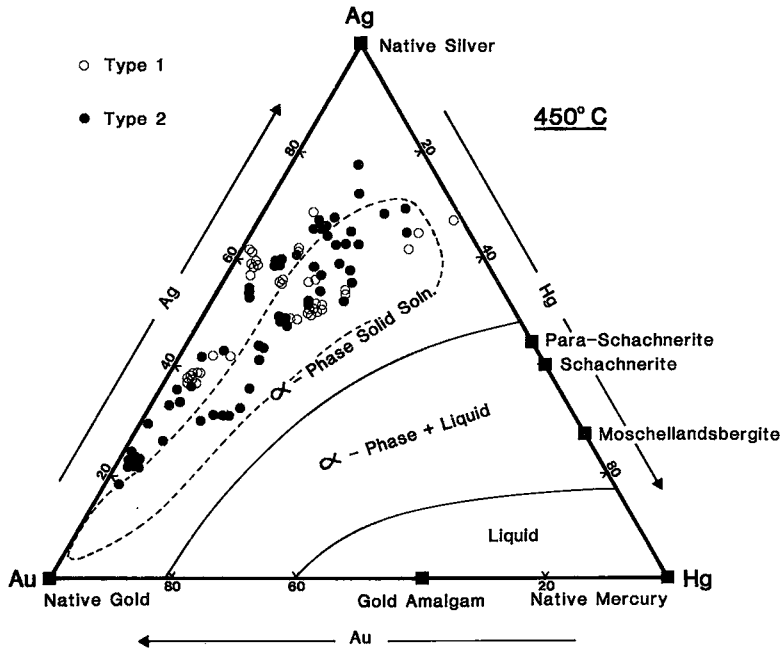

FIG. 5. Schematic 450°C isothermal section of the Ag–Au–Hg ternary system (in wt.%). The phase boundaries for the α-phase are redrawn from Basu *et al.* (1981). The composition of several naturally occurring binary alloys with the discrete stoichiometric compositions of intermetallic compounds (*e.g.*, moschellandsbergite) is projected from lower temperatures onto the section, whereas that of the three pure native metals is shown at the apices. The field of known compositions as compiled by Shikazono & Shimizu (1988) is shown with a dashed line. The composition from the 104 microprobe analyses of Trout Lake Au–Ag–Hg alloy are designated by type and plotted.

to be due to metallic Fe dissolved in the Au–Ag–Hg alloy.

The inclusion of an extraneous sulfide component in the analyses does not affect the relationship among Au, Ag and Hg, which are of prime interest in our investigation. Consequently, all data were considered. Eight representative compositions of the Trout Lake Au–Ag–Hg alloy, which cover the observed range in elemental concentrations, are given in Table 2. The complete set of 104 compositions are plotted on a Ag–Au–Hg triangular diagram in Figure 5, and have been submitted to the Depository of Unpublished Data, CISTI, National Research Council of Canada, Ottawa, Ontario K1A 0S2.

THE Ag–Au–Hg TERNARY SYSTEM

Previous studies have shown that most compositions of naturally occurring alloys of these three elements are related into the Ag–Hg, Au–Hg and Au–Ag binary systems. However, Scott (1977), Nazmova & Spiridonov (1979), Ozerova *et al.* (1980), Basu *et al.* (1981), Nysten (1986), Harris (1986), Shikazono & Shimizu (1988) and others have reported naturally occurring alloys of Ag and Au with minor to major concentrations of Hg. These ternary alloys correspond to the α-phase binary solid-solutions of the three binary systems extended into the ternary system Ag–Au–Hg.

In the absence of experimental work on the ternary system Ag–Au–Hg, Basu *et al.* (1981) relied on the three binary systems Ag–Au, Ag–Hg and Au–Hg to estimate the stability field for the face-centered (*fcc*) ternary α-phase. The β-phases Ag_5Hg_4 and Au_7Hg_3, observed in the corresponding binary systems, are stable below 276 and 419°C, respectively. No such β-phase is observed in the binary system Ag–Au; therefore, below 419°C, features near the Hg-rich apex of the ternary system are uncertain. Thus Basu *et al.* (1981) constructed a schematic 450°C isothermal section of the ternary system that shows the extrapolated field of stability of the α-phase, presuming no other ternary solid phase (Fig. 5).

The metamorphic grade at Trout Lake corresponds to middle greenschist facies; being above

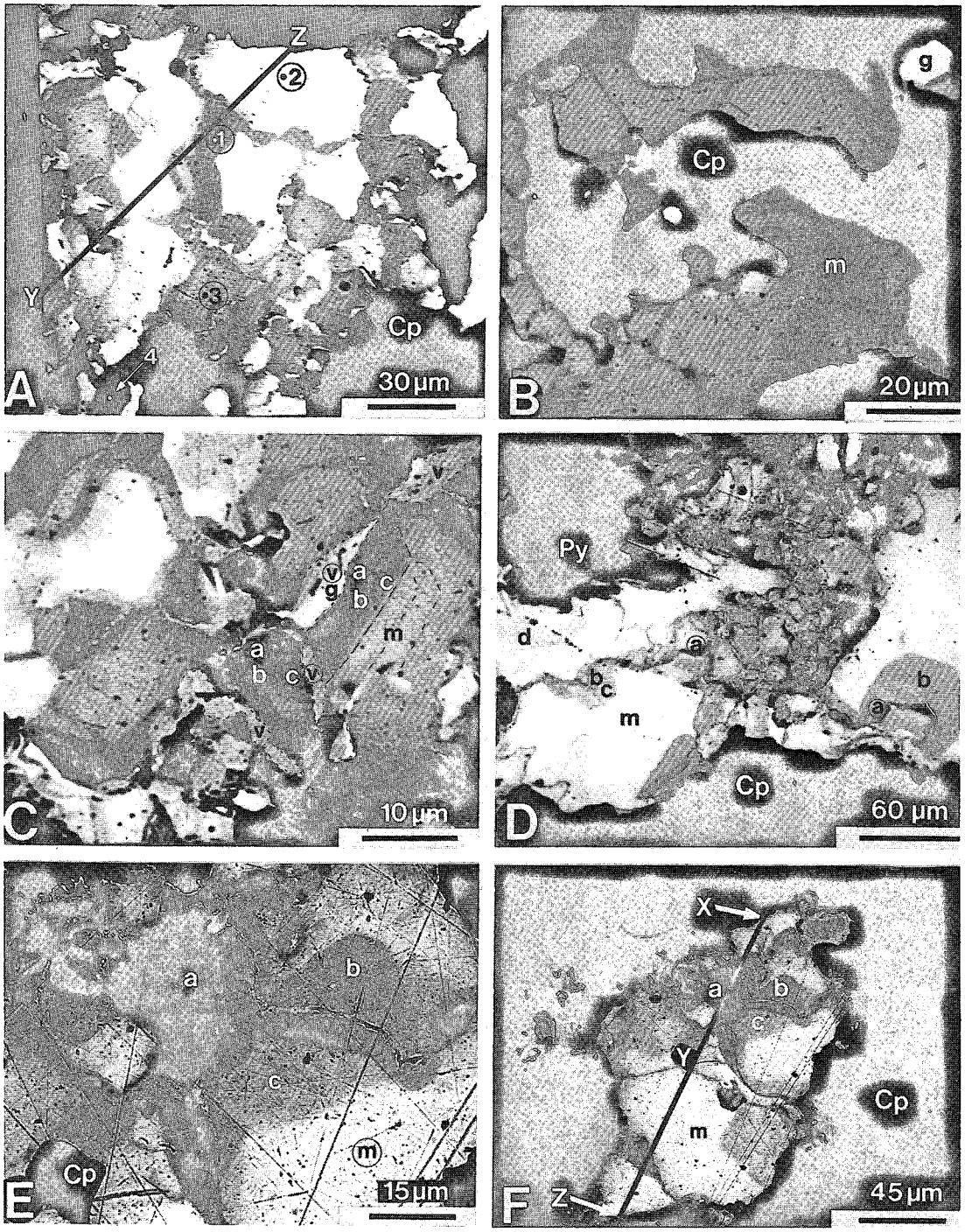

FIG. 6. High-contrast BSE photographs of Type-2 Au–Ag–Hg alloy: (A) TLN.1–98i: inhomogeneous mass of alloy showing location of analytical points 1 to 4 presented in Table 3, and location of a major segment (Y to Z) of the wavelength-dispersion traverse (X to Z) shown in Fig. 7A; (B) TLN.1–89i: fine-grained, discrete grains of Au-rich alloy (g) enveloped in alloy of intermediate composition (m); (C) TLN.1–89i: complex zoning in alloy, consisting of oscillatory zoning at "m", separated from a strongly zoned Ag-rich rim by a resorption edge, and cross-cut by a veinlet of

the biotite isograd indicates that temperatures reached at least 400°C (Aggarwal & Nesbitt 1987). Furthermore, as is shown later, we consider the crystallization of the Au–Ag–Hg alloy to be an essentially retrograde process. Extrapolation of the system Au–Ag–Hg to lower temperatures, assuming no other ternary phases in the Hg-poor region of the system, indicates only minor shrinkage of the stability field of the α-phase. Therefore, the schematic 450°C isothermal section is a reasonable model for the crystallization of Au–Ag–Hg alloy at Trout Lake.

The compositions of Trout Lake Au–Ag–Hg alloy are plotted on the section, and form a large field with a general trend of slightly increasing Hg with increasing Ag, and decreasing Au. Nazmova & Spiridonov (1979), Nysten (1986) and Shikazono & Shimizu (1988) also have observed this compositional trend, which conforms with the increased solubility of Hg in the Ag end-member. The compositions all plot within the α-phase stability field, and are thus analogous to the *fcc* α-phase solid solution of Basu *et al.* (1981). Furthermore, the compositions span much of the field of known compositions compiled by Shikazono & Shimizu (1988), and extend the field for compositions near the Au–Ag join and Ag apex (Fig. 5). The large range in compositions observed in this study is attributed to the selection of analytical points on the basis of features visible in high-contrast BSE imagery, which allows analysis of otherwise obscured extreme compositions.

Zoning and Distribution of Type-2 Au–Ag–Hg Alloy

Basu *et al.* (1981) and Nysten (1986) also have reported considerable inhomogeneity over distances of fractions of micrometers within grains of Au–Ag–Hg alloys. The high-contrast BSE photographs in Figures 6A to F illustrate the extreme compositional inhomogeneity in masses of Type-2 alloy. Points 1 to 4 in Figure 6A correspond to the analytical data in Table 3, which were generated in order to confirm the compositions of grains having different levels of grey in the BSE images of Au–Ag–Hg alloy masses. It is apparent from Table 3 that the brightest grains have the highest Au and Hg contents, whereas the darkest grains are Ag-rich. Thus, whereas the complete set of 104 analyses gives a trend of increasing Hg with increasing Ag, these four analyses from a single mass show Ag inversely related to both Hg and Au. Element profiles across masses of Type-2 alloy consistently show the antipathetic relationship of Ag to Au and Hg (Fig. 7). This relationship suggests a trend toward progressively Ag-rich late compositions at the expense of both Au and Hg, where only the initial composition of each mass parallels the trend of increasing Hg with Ag. Nonetheless, because Au and Hg have a similar atomic number (79 and 80, respectively) much greater than that of Ag (47), the BSE signal and the points selected on the basis of it may not wholly describe the general trend in compositional variation.

In general, within masses of Type-2 Au–Ag–Hg alloy, high-Au compositions occur as rare grains (≤ 10 μm) enveloped in more intermediate compositions (Fig. 6B), the interstices of which are infilled by Ag-rich compositions. In Figure 6C, several grains show pronounced zoning. In subidiomorphic grains, *e.g.*, "m", zoning is parallel to crystal faces. This strong crystallographic control confirms that the range in compositions constitutes solid solution within the extrapolated α-phase stability field of Basu *et al.* (1981), and is not due to separate phases produced by subsolidus unmixing. The latter had been postulated in the absence of high-contrast BSE imagery by Basu *et al.* (1981) and Nysten (1986) to explain the inhomogeneity in X-ray dot images. The core of the grain indicated by "m", which contains oscillatory zoning, is separated from a strongly zoned Ag-rich (dark) rim by a boundary resembling a resorption edge. The grain is cross-cut by a veinlet of intermediate composition "v", that contains trails of blebs of Au-rich composition "g" (bright white). These features indicate distinct breaks in the conditions of crystallization, with only partial re-equilibration. In contrast to the general tendency for the later-stage compositions to be Ag-rich, here the final composition "g" is relatively Au-rich. This composition may be the homogenized product of earlier compositions being redissolved during a localized deformational event, rather than a reversal of the typical sequential crystallization of Ag-rich compositions.

The mass of Type-2 Au–Ag–Hg alloy in Figure 6D contains a central zone of fractures that are lined by Ag-rich compositions, which contrast with the earlier homogeneous intermediate composition "m". Four distinct generations occurring as zones of progressively Ag-rich compositions are observed, with increasing Ag content toward the center of the frac-

intermediate composition "v" that contains trails of blebs of Au-rich composition "g"; (D) TLN.1–89k: large mass of alloy showing episodic diffusion-induced zoning of Ag and Hg (a, b, c and d) into earlier intermediate composition (m) along fractures; (E) TLN.1–89b: inhomogeneous mass of alloy, showing episodic diffusion-induced zoning of Ag (a, b and c) along fractures into earlier intermediate composition (m); (E) TLN.1–89b: lower-magnification view of mass in E, showing location of the wavelength-dispersion traverse (X to Z) shown in Fig. 7B, and relation to fractures lined by progressively more Ag-rich compositions.

TABLE 3. CHEMICAL COMPOSITION OF Au-Ag-Hg ALLOY IN SECTION TLN.1-89I (MICROPROBE DATA)

Wt.%	Ag	Au	Hg	Fe	Total.
1.	72.61	14.09	14.26	nd.	100.96
2.	54.11	22.91	21.16	nd.	98.18
3.	64.19	18.68	16.08	nd.	98.95
4.	76.47	11.17	11.14	nd.	98.78

Analytical parameters as in Table 2.
See Figure 6A for location of points.

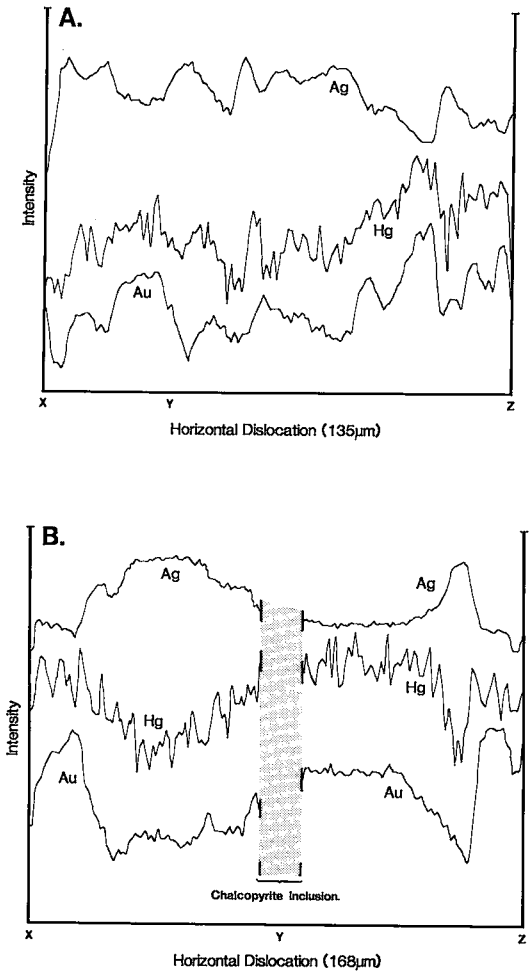

FIG. 7. Profiles of Au, Ag and Hg concentrations across a mass of Type-2 Au–Ag–Hg alloy in (A) TLN.1-89i, and (B) TLN.1-89b, showing antipathetic relationship of Ag to both Au and Hg. Continuous, qualitative, wavelength-dispersion traverse. Location of traverses shown in Fig. 6A and E.

tures. A similar pattern of three late Ag-rich zones also is seen in Figures 6E and F. This texture is interpreted as due to the episodic diffusion of Ag into the earlier-formed more intermediate composition.

The contact between laminae of massive chalcopyrite and chlorite schist, along which Type-2 Au–Ag–Hg alloy is concentrated, is enriched in clausthalite and naumannite, and contains abundant quartz, calcite, biotite, monazite and particularly coarse-grained ($\leq$1 cm) plagioclase within a relatively homogeneous bleached zone of recrystallized matrix chlorite. The plagioclase is variably replaced (commonly occurs as pseudomorphs) by a fine-grained clay mineral (tentatively identified as smectite) and an associated rim of fine-grained adularia. The timing of the clay alteration with respect to the crystallization of Au–Ag–Hg alloy is not clear, as there is no close spatial association of the clay with the alloy, though the clay corrodes chalcopyrite. Pyrite, chalcopyrite, sphalerite and pyrrhotite are invaded and corroded by Type-2 Au–Ag–Hg alloy. The pyrite is also deformed and partially altered to marcasite, which is characteristic of late-stage parageneses associated with the replacement of pyrite in shear zones. Furthermore, marcasite, clausthalite, rucklidgeite and hessite have been observed as interstitial phases associated with Type-1A Au–Ag–Hg alloy. These observations are generally consistent with the paragenesis of gold associated with pyrite, tellurides, quartz and carbonate in discordant veinlets, representing the remobilized fractions in Archean gold deposits (Springer 1983), and suggests that Au, Ag, Hg, Pb, Se, Te, Si, K, Ca and Na were introduced along this contact *via* a fluid phase.

GEOCHEMICAL ASSOCIATION OF GOLD

Bulk chemical analyses were carried out for 19 chalcophile elements in 27 representative samples of the nine ore types (Healy & Petruk 1988). Correlation and factor analysis of the chemical analyses failed to identify any significant geochemical association of Au with the other 18 elements, even though positive covariance with Cu and As was expected. Company geologists have observed a correlation between Au and Cu in production assays for the Cu-rich footwall ores, and this correlation is confirmed by petrographic observations of large masses (*i.e.*, $\leq$5 mm) of Type-2 alloy in the Chalcopyrite Stringer ores. Importantly, samples TLN.1-89, TLN.2-11 and TLN.2-8, which are Cu-rich and contain abundant alloy, were not included in the small suite of samples (*i.e.*, n = 27) for which chemical analyses for Au were done. This suite was selected by Healy & Petruk (1988) on criteria other than those necessary to establish a Au–Cu trend, and is biased away from high-gold samples. Thus the Au assays are not wholly representative of this typically lognormally distributed element, which also is characterized by the "nugget" or "particle sparsity" effect.

Gold is commonly associated with arsenian pyrite and arsenopyrite in many types of deposits (Wells & Mullens 1973, Boyle 1979, Springer 1983, Gasparrini 1983, Cook & Chryssoulis 1989). Arsenopyrite is the principal As-carrier in the Trout Lake ore and is most abundant in the hanging-wall Layered Pyrite + Sphalerite ore type, but this ore is not enriched in Au.

The Au/Ag ratio of the deposit is 0.11 (*i.e.*, 1.73 ppm Au and 15.87 ppm Ag; Ko 1986), whereas that of the Au–Ag–Hg alloy is 0.82 (*i.e.*, 38.68% Au and 49.22% Ag). The Au–Ag–Hg alloy is the principal Au-bearing mineral, but accounts for a maximum of only 15% of the Ag. Therefore, any Au–Ag correlation due to Au–Ag–Hg alloy is masked by the Ag in other minerals. The ore contains 19.3 ppm Hg (Healy & Petruk 1989), but the Au/Hg ratio in Au–Ag–Hg alloy is 3.52, and therefore accounts for a maximum of only 3% of the Hg in the deposit. Both Ag and Hg occur in concentrations that are approximately an order of magnitude greater than that explained by their occurrence in the Au–Ag–Hg alloy. This contributes to the lack of significant covariance in Ag and Hg with Au.

The principal hosts of Ag and Hg were estimated from material-balanced chemical assays and mineral quantities of known (Table 1) and inferred Ag- and Hg-bearing minerals in the Trout Lake concentrator products (Healy & Petruk 1989). They estimated that sulfosalts (principally freibergite and pyrargyrite) and tellurides account for <24%, and Au–Ag–Hg alloy, for <19% of the Ag in the ore. In the absence of direct measurement, chalcopyrite, pyrite, sphalerite and galena were also estimated to contain approximately 45, 11, 55 and 750 ppm Ag, respectively, corresponding to 23, 14, 19 and 3%, respectively, of the Ag in the ore. Subsequently, Pinard & Petruk (1989) determined by microprobe analysis that the average Ag-content of Trout Lake galena is 660 ppm. Except for Au–Ag–Hg alloy, no other Hg-bearing mineral was identified by Healy & Petruk (1989); we infer that pyrite and sphalerite contain approximately 85 and 120 ppm Hg, respectively, corresponding to 66 and 31%, respectively, of the Hg in the ore.

"Invisible" Gold

"Invisible" Au is that which cannot be observed by optical or electron microscopy, which may occur either in solid solution or as submicrometer inclusions in sulfide minerals, and which cannot be recovered directly by cyanidation (Chryssoulis *et al.* 1987). Romberger (1986) and Huston & Large (1989) postulated that coprecipitation with pyrite of Au carried in solution as bisulfide complexes would generate significant submicroscopic grains of gold in pyrite. Furthermore, Boyle (1979) postulated that high-temperature pyrite and arsenopyrite take up Au and Ag largely as structural constituents, which tend to exsolve on cooling. The Au and Ag diffuse to fractures and grain boundaries, where alloys of Au and Ag crystallize. Boyle (1979) also suggested that the frequent occurrence of "invisible" Au in ores is due to retention of Au and Ag as structural constituents in relatively unfractured and unrecrystallized pyrite and arsenopyrite. Relatively unfractured pyrite metablasts, embedded in a "soft" matrix of sphalerite, are common in several ore types in which only rare grains of Au–Ag–Hg alloy were observed (*e.g.*, Layered Pyrite + Sphalerite). Conversely, abundant Au–Ag–Hg alloy was observed in Sheared Chalcopyrite + Sphalerite and Chalcopyrite Stringer ore types, where pyrite has typically undergone intense cataclastic deformation and has been partly to completely broken down.

Several lines of evidence, including data obtained by electron and ion microprobes, and results of various metallurgical analyses, show that in both natural and synthetic systems, significant "invisible" Au (*i.e.*, 1 to 1000 ppm) is bound in pyrite and arsenopyrite (Wells & Mullens 1973, Boyle 1979, Hausen 1981, Springer 1983, Chryssoulis *et al.* 1987, Cook & Chryssoulis 1989, Cabri *et al.* 1989). Approximately 30% of the Au in the Trout Lake ore is routinely lost to the tailings during standard froth flotation (Healy & Petruk 1989). Laboratory flotation tests of the tailings (Milojokovic 1983, McEachern 1987) have shown that at least 78% of the Au in the tailings is associated with pyrite and arsenopyrite. Cyanidation of a tailings sample (without regrinding) recovered 30% of the gold, and cyanidation after regrinding to 80% finer than 18 μm recovered 64% of the gold in the tailings. Thus, 36% of the Au in this sample of the tailings is assumed to occur as "invisible" gold in pyrite and arsenopyrite.

The Au content of arsenopyrite, and the Au and As content of pyrite in the above cyanide-tested sample of tailings, were determined by grain-discrete analysis of these minerals using secondary ion mass spectrometry (SIMS). The SIMS technique was described by Chryssoulis *et al.* (1987). The Au concentrations in 46 pyrite grains vary from 0 to 6.80 ppm, with a mean value of 0.72 ppm. The As concentrations in the same grains vary from <10 to 4100 ppm, with a mean value of 500 ppm. The Au and As concentrations show no significant positive covariance. The Au concentrations in 44 arsenopyrite grains vary from 2 to 112 ppm, with a mean value of 30.2 ppm. The distribution of "invisible" Au in pyrite and arsenopyrite, and of As in pyrite, is shown as histograms in Figure 8. The complete set of SIMS analytical data have been submitted to the Depository of Unpublished Data, CISTI, National Research Council of Canada, Ottawa, Ontario K1A 0S2.

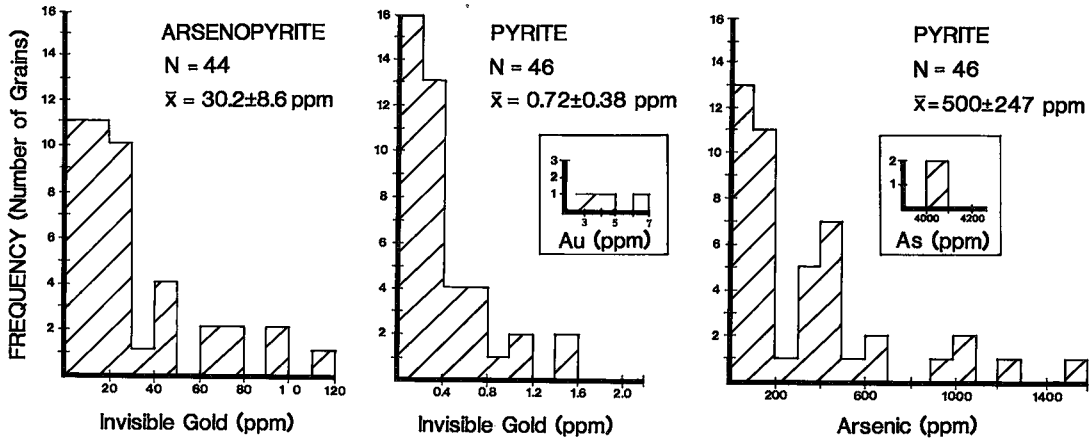

FIG. 8. Histograms displaying the distribution of Au concentrations in arsenopyrite, and the Au and As concentrations in pyrite, as determined by SIMS analyses of these minerals in a sample of Trout Lake concentrator tailings.

DISTRIBUTIONS OF Au–Ag–Hg ALLOY AND OF "INVISIBLE" GOLD

The SIMS data and mineral quantities determined by image analysis for pyrite (*i.e.*, 25%) and arsenopyrite (*i.e.*, 0.2%) in the cyanide-tested sample of tailings show that the "invisible" Au in pyrite and arsenopyrite contributes 0.18 and 0.06 ppm, respectively, to the 0.67 ppm Au assay in the tailings. Thus, approximately 27% of the Au in this sample of tailings is due to "invisible" Au in pyrite and 9% in arsenopyrite, and fully accounts for the 36% of the Au not recovered by cyanidation.

Healy & Petruk (1989) sampled products from the Trout Lake concentrator circuit over a two-hour period. A material-balance procedure adjusted the chemical assays and modal abundances, and simultaneously calculated recoveries of these at each point in the circuit under simulated steady-state conditions. We determined that 59, 15 and 26% of the Au was recovered in the Cu-concentrate, Zn-concentrate and tailings, respectively. Fractions of the bulk-Au assay in the end products due to pyrite and arsenopyrite were calculated using the material-balance-adjusted modal quantities and "invisible" gold contents of these minerals. This assumes that the "invisible" gold contents of pyrite and arsenopyrite are identical to those determined by SIMS on the separate sample of tailings, and thus that the distribution of "invisible" gold corresponds to the distribution of these minerals. Pyrite and arsenopyrite were assigned gold assays of 0.12 and 0.02 ppm Au in the feed, and account for 6 and 1%, respectively, of the Au in the feed. Similarly, pyrite and arsenopyrite account for 20 and 2%, respectively, of the Au in the tailings (Table 4).

Gold due to Au–Ag–Hg alloy was calculated by subtracting the Au assay assigned to pyrite and arsenopyrite from the bulk-Au assay of each end product. Fractions of the bulk-Au assay in the feed thereby assigned to each mineral indicate that Au–Ag–Hg alloy accounts for 93% of the Au in the feed, with pyrite and arsenopyrite accounting for only 6 and 1%, respectively. Recoveries of Au–Ag–Hg alloy also were calculated on the basis of the distribution of the Au assay assigned to the alloy in each product, and indicate that 63, 16 and 21% of the alloy are recovered in the Cu-concentrate, Zn-concentrate and tailings, respectively (Table 4). A search for the Au–Ag–Hg alloy, using an EDS-assisted image-analyzer-search routine that detects grains larger than 1.5 μm in diameter (Petruk 1988), failed to find any grains of the alloy in the tailings. This indicates that in the tailings, the alloy is present in grains smaller than 1.5 μm.

The recovery of "invisible" Au, which accounts for approximately 7% of the Au in the feed, is assumed to correspond to the recovery of pyrite plus arsenopyrite. Hence, 5 and 7% of the "invisible" Au are assumed to have been recovered in the Cu-concentrate and Zn-concentrate, respectively, with the remaining 88% having been rejected to the tailings.

DISCUSSION

In order to explain the distribution of Au in volcanogenic massive sulfide deposits, Huston & Large (1989) proposed a model for the transport and deposition of Au that is consistent with the models for the evolution of the hydrothermal system of Eldridge *et al.* (1983) and Pisutha-Arnond & Ohmoto (1983).

TABLE 4. BULK Au ASSAYS, AND MODAL ABUDANCES AND Au ASSAYS ASSIGNED TO PYRITE, ARSENOPYRITE AND Au-Ag-Hg ALLOY IN THE FOUR END PRODUCTS OF THE TROUT LAKE CONCENTRATOR CIRCUIT

PRODUCT	GOLD		MODAL ABUNDANCES AND ASSIGNED Au ASSAYS*				ASSIGNED Au ASSAYS DUE TO, AND RECOVERY OF Au-Ag-Hg ALLOY**	
			PYRITE		ARSENOPYRITE			
	Assay (ppm)	Recovery (%)	Mod Abds. (Wt.%)	Assay (ppm)	Mod Abds. (Wt.%)	Assay (ppm)	Assay (ppm)	Recovery (%)
Feed	2.23	100.0	15.4	0.12	0.06	0.02	2.00	100
Cu-Concentrate	18.7	59.2	10.4	0.07	0.10	0.03	18.6	63
Zn-Concentrate	7.58	15.3	12.3	0.09	0.45	0.14	7.35	16
Tailings	0.65	25.6	17.2	0.13	0.03	0.01	0.51	21

Note: Bulk Au assays and modal abundances of pyrite and arsenopyrite are material-balance adjusted (data from Healy & Petruk 1989).

* Au assays assigned to pyrite and arsenopyrite are based on the modal abundances of these minerals as determined by image analysis, and their average Au content i.e., pyrite ($\bar{x}$ = 0.72 ppm Au) and arsenopyrite ($\bar{x}$ = 30.2 ppm Au) as determined by SIMS.

** Au assays due to, and recoveries of, Au-Ag-Hg alloy are estimated by subtracting the Au assay assigned to pyrite and arsenopyrite from the bulk Au assay of the product.

According to this model, Au is transported as chloro- and thio-complexes, the dominance of which varies temporally and spatially within the hydrothermal cycle. The association of Au with Zn–Pb–Ag in the upper and outer parts of Zn-rich lenses is attributed to the transport of Au as the bisulfide complex $Au(HS)_2^-$, whereas the association of Au with Cu in the stringers and at the bases of Cu-rich lenses is attributed to transport as the chloride complex $AuCl_2^-$. At Trout Lake, the predominant association of Au with the Cu-rich, footwall, massive sulfide and stringer ores suggests that Au transport as chloride complexes in relatively hot (>300°C) fluids dominated, whereas transport as bisulfide complexes in cooler (<300°C) fluids passing to the marginal and upper Zn-rich parts of the lenses was subordinate. The distribution of Au at Trout Lake largely reflects this premetamorphic hydrothermal history, though significant local migration of the Au during metamorphism, a process suggested by Romberger (1986), is clearly indicated.

Huston & Large (1989) postulated that Au transported as chloride complexes is precipitated by decreasing temperature or increasing pH and, therefore, is not intimately associated with sulfide minerals, but occurs as coarse free grains. Romberger (1986) and Huston & Large (1989) argued that precipitation of Au from bisulfide complexes is most efficient by decreasing total reduced sulfur (ΣS), either by oxidation or coprecipitation with sulfides such as pyrite. The latter process would produce significant submicroscopic or "invisible" Au in pyrite. Therefore, this model is consistent with the occurrence of Au at Trout Lake; the probable deportment of Au in the premetamorphic deposit, when subjected to recrystallization and local migration during metamorphism, is apt to generate Type-1 Au-Ag-Hg alloy dominantly in the hanging-wall ores, and Type-2 alloy in the stringer ores.

Fluid conditions [*e.g.*, salinity, pH and $f(O_2)$] during regional metamorphism of volcanogenic massive sulfide deposits differ significantly from those prevailing in the fluids that precipitate the sulfides on or immediately below the seafloor. Textures and mineral assemblages at Trout Lake (Healy & Petruk 1988) indicate that conditions during peak and retrograde metamorphism are consistent with pore fluids of moderate to low temperature ($\leq$400°C) and oxidation state [log $f(O_2)$ of –35 to –45], near-neutral pH and low salinity. Under these conditions, bisulfide complexes [*e.g.*, $Au(HS)_2^-$, $Ag(HS)_2^-$, $Hg(HS)_2^{2-}$] are the dominant carriers of Au, Ag and Hg in aqueous solution (Seward 1984, Cathles 1986, Romberger 1986, Shikazono & Shimizu 1987, Sugaki *et al.* 1987, Wells & Ghiorso 1988). The most efficient mechanisms for deposition from these solutions are a decrease in ΣS for Au (Seward 1984, Romberger 1986), changes in pH or a decrease in ΣS for Ag (Sugaki *et al.* 1987), and boiling and a decrease in ΣS for Hg (Wells & Ghiorso 1988). Boiling (not important under greenschist-facies metamorphism), precipitation of sulfides, dilution and oxidation are effective processes for decreasing ΣS in the fluid (Seward 1984). Textures such as the alteration of pyrrhotite to pyrite–magnetite symplectite and "bird's-eye"-textured pyrite–marcasite (Healy & Petruk 1988) indicate slightly increasing oxidation states during retrograde metamorphism, whereas the presence of calcite, adularia and argillic alteration (associated with Type-2 alloy) indicate neutral to alkaline pH (Romberger 1986).

The most likely causes of Au, Ag and Hg precipitation from metamorphic pore-fluids at Trout Lake are: (1) decrease in ΣS of the fluid due to continued crystallization of sulfides, and increase in $f(O_2)$; (2) decrease in temperature during retrograde metamorphism, and (3) adsorption and reduction of Au, Hg (Bancroft & Jean 1982, Jean & Bancroft 1985, 1986) and possibly Ag onto pyrite grains or sheet silicates. Although the solubility of the Au bisulfide complexes decreases with increasing temperature, changes in other temperature-dependent variables [*e.g.*, $f(O_2)$ and ΣS] result in increasing "geological" solubility of Au with temperature to 300°C, above which the

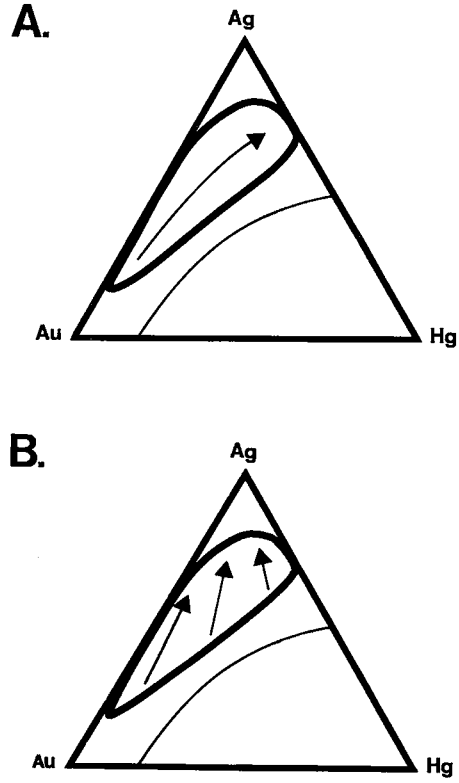

FIG. 9. Schematic triangular diagram showing the field of Trout Lake Au–Ag–Hg alloy compositions (in wt.%) and two possible trends in composition of alloys crystallizing in paragenetic sequence: (A) later compositions are Ag- and Hg-rich, paralleling the general trend of the field; and (B) later compositions are progressively Ag-rich and Au- and Hg-poor.

solubility falls off sharply (Cathles 1986). In addition, the solubility of Ag bisulfide complexes is less sensitive to decreasing temperature than that of Au and Hg (Cathles 1986, Barnes *et al.* 1967, Sugaki *et al.* 1987). Thus, the adsorption of Au and Hg by pyrite, the more rapid decrease in the solubilities of Au and Hg bisulfide complexes with falling temperature and slightly increasing oxidation state, and the generally wider range in fluid conditions under which Ag bisulfide complexes are soluble (Hannington & Scott 1988), may tend to generate higher Ag/Au and Ag/Hg activity ratios in evolving pore fluids during retrograde metamorphism. Furthermore, we interpret that 97% of the Hg in the ore is structurally bound in pyrite (66%) and sphalerite (31%), both of which are relatively refractory sulfides. The difference in the covalent radii of Hg (1.49 Å), Au and Ag (1.34 Å), as compared to that of Fe (1.17 Å), may preferentially retard the diffusion of Hg in pyrite (Puddephatt 1972). Because Au and Ag are released from pyrite by solid-state diffusion (Boyle 1979), the availability of Hg in the pore fluids is thus constrained.

Hannington & Scott (1988) noted that Ag is transported under similar fluid conditions to those of Au, but the solubility of Ag occurs over a wider range of temperature, pH and salinity. This difference in solubility may generate a broader distribution and less specific host mineralogy for Ag in the premetamorphic deposit. Nonetheless, coprecipitation is probably a major depositional process for Ag transported as bisulfide complexes, thereby leading to high concentrations of Ag in the principal sulfides pyrite, chalcopyrite and sphalerite. The subsequent metamorphic recrystallization of the principal sulfides would then play an important role in the availability of Ag in the pore fluids, though Healy & Petruk (1989) have inferred that these sulfides have retained high concentrations of Ag. However, as the number of inferred and known Ag-bearing minerals at Trout Lake is large (12), the determination of the pre- and peak-metamorphic sites of Ag is highly speculative.

The general trend of increasing Hg with Ag shown in Figure 5 is not reflected in the composition of alloys crystallizing in successively later generations. Profiles of element concentration across masses of Type-2 alloy consistently show the sympathetic variation of Au and Hg concentrations (Fig. 7). This relationship is observed in masses of alloy that are predominantly of the earliest (Fig. 7A) and final (Fig. 7B) compositions. The general trend of the compositional field merely reflects the increasing solubility of Hg in the Ag end-member, rather than a sequence toward later Ag- and Hg-rich compositions (Fig. 9A). Thus the element profiles across masses containing paragenetically distinguishable features show that the sequence in compositional variation is consistent with increasing Ag/Au and Ag/Hg activity ratios, leading to precipitation of progressively Ag-rich compositions (Fig. 9B).

The specific association of Au with pyrite in numerous types of deposits (Wells & Mullens 1973, Boyle 1979, Springer 1983, Romberger 1986) suggests that Au is precipitated either by coprecipitation from bisulfide complexes (Romberger 1986, Huston & Large 1989), or by surface adsorption and reduction onto pyrite grains (Bancroft & Jean 1982, Jean & Bancroft 1985), rather than by decreased solubility related to falling temperatures of the fluids. Both these processes explain the high local concentrations of Au with pyrite, and also obviate the need for hydrothermal solutions saturated with Au (Seward 1984, Jean & Bancroft 1985, Romberger 1986). The localized concentration of Au in extremely specific textural types at Trout Lake suggests preferential precipitation of Au at these sites. These sites are areas

of potential Au adsorption and reduction by pyrite or sheet silicates, or areas of low stress and strain favoring the precipitation of dissolved components in the metamorphic pore-fluids. In the case of Type-1 Au–Ag–Hg alloys, the dilated fractures and grain boundaries of pyrite porphyroclasts may behave as "pressure shadows". Diffusion of Au, Ag and Hg to these sites through pyrite grains, as suggested by Boyle (1979), may assist nucleation of the Au–Ag–Hg alloy.

The distribution and localized abundance of Type-2 Au–Ag–Hg alloy are clearly inconsistent with the process suggested by Boyle (1979). It is improbable that these localized concentrations of Au–Ag–Hg alloy were concentrated by solid-state diffusion from pyrite (*i.e.*, 0.2 area% Au–Ag–Hg alloy and 5.25 area% pyrite in TLN.1-89a) or any of the surrounding sulfides, or by plastic flow. Wilson & Rucklidge (1987) and Springer (1985) emphasized the importance of hydrothermal conduits as structural factors controlling the deposition of Au in Archean gold deposits. The contact along which Type-2 Au–Ag–Hg alloy is preferentially concentrated must have acted principally as a locus for high fluid-flow, along which Au-, Ag- and Hg-bearing solutions migrated. Low stress and strain associated with a dilational contact within the nose of a fold may have generated chemical potential gradients favoring the precipitation of Au from the fluid phase. Importantly, the noncrystalloblastic nature of these alloys, combined with the idiomorphic character of the oscillatory zoning in Figure 6C, strongly suggest open-space growth.

The compositions of Type-2 Au–Ag–Hg alloy (Fig. 5) span virtually the entire compositional field of Trout Lake alloy. We suggest that Types 1 and 2 formed by a combination of solid-state diffusion to the margins of pyrite grains (Boyle 1979), coupled with dissolution, local migration and precipitation at preferred sites from late metamorphic pore-fluids enriched in Au, Ag and Hg. However, much of the Type-2 Au–Ag–Hg alloy probably formed exclusively by hydrothermal remobilization of coarse free "gold" in the Cu-rich footwall ores. The lack of compositional distinction between Au–Ag–Hg alloy Types 1 and 2 requires at least that Type 1 equilibrated with the pore fluids, even if migration was minimal. However, the Type-1 Au–Ag–Hg alloy that occurs as fine-grained inclusions in pyrite, and that could not be quantitatively distinguished on the basis of composition, may have formed solely by solid-state diffusion (Boyle 1979). Sample TLN.2-8, which contains 103 grains of Type-1A Au–Ag–Hg alloy (Figs. 1 A–D), was taken from adjacent to a syntectonic quartz diorite sill. The abundance of alloy in this sample seems more readily explained by locally induced remobilization of the ores and widespread breakdown and replacement of pyrite near the sill (Healy & Petruk 1988) than by solid-state diffusion. Similarly inconsistent with the latter process is the localized abundance of Type-1B Au–Ag–Hg alloy in TLS.3-40 (Figs. 2C, D). For the solid-state diffusion process of Boyle (1979), we calculate that this cluster requires that Au diffused from up to 1 cm away in massive pyrite. Such an extended diffusion path for Au across numerous pyrite grains is in sharp contrast to the inhomogeneity (over distances of micrometers) of the Au–Ag–Hg alloy grains, which suggests sluggish solid-state diffusion of Au, Ag and Hg even within the metallic framework of the alloy itself. However, the latter was formed at temperatures below the peak of metamorphism, subsequent to pyrite metablastesis.

The distinctive association of Type-1B Au–Ag–Hg alloy with freibergite, galena, sphalerite and minor arsenopyrite is similar to that of Au associated with sphalerite, galena and Ag-bearing sulfosalt assemblages in the Southern Explorer Ridge (Hannington & Scott 1988). Huston & Large (1989) also have identified the association of Au with Zn–Pb–Ag in massive sulfide and other types of deposit. These studies attribute this association to precipitation of Au from bisulfide complexes in low-temperature (<300°C) fluids. In addition, Seward (1984) and Romberger (1986) speculated on the possible role of thioarsenide (and thioantimonide) complexes in the transport of Au in hydrothermal solutions. Transport and deposition from fluids containing these complexes are likely to generate assemblages similar to Type 1B. However, it is also probable that as the crystallization of Au–Ag–Hg alloy is considered retrograde, the alloy would be preferentially associated with other late-stage lower temperature phases crystallizing in available fluid conduits within Zn–Pb–Ag-rich ores.

We contend that the oscillatory zoning in Figure 6C represents preserved growth-related zoning produced by equilibration of the evolved fluid composition in the matrix with the edge of the growing grain. This equilibration would have occurred below the peak metamorphic temperature and activity of Au. This texture is not preserved in other sections, suggesting homogenization by intracrystalline volume-diffusion (Schmalzried 1974). Oberthur & Saager (1986) suggested that volume diffusion caused the pervasive homogenization of the Au–Ag–Hg alloy of the Witwaterstrand placer gold deposits during lower-greenschist-facies metamorphism. However, unlike the placer "gold" grains in the Witwaterstrand deposits, the Au–Ag–Hg alloy grains at Trout Lake would not have been available during the extensive period of prograde metamorphism.

The zoning illustrated in Figures 6A, C, D, E and F suggests diffusion-induced zoning (Loomis 1983), where the grains of intermediate composition have Ag-rich compositions imposed on them by diffusion

from grain surfaces that are in contact and equilibrating with the interstitial fluid. The episodic character of the late Ag-rich compositions may reflect changes in the activity of $Ag(HS)_2^-$ related to the crystallization of low-temperature Ag-bearing sulfides and sulfosalts. As these phases crystallize, competing equilibrium reactions such as (1) $Au(HS)_2^- + Ag^\circ = Ag(HS)_2^- + Au^\circ$; (2) $Ag(HS)_2^- + \frac{1}{2}H_2 = Ag^\circ + H_2S + HS^-$; and (3) $Ag(HS)_2^- = \frac{1}{2}Ag_2S + \frac{1}{2}H_2S + HS^-$ may have generated stepwise changes, and possibly minor reversals in the general trend of increasing activity of Ag° in the alloy.

The configuration of the diffusion-induced zoning is largely controlled by grain boundaries in Figures 6A and C, and by regions of dislocations bounding fractures in Figures 6D, E and F. In these regions of the grains, diffusion mechanisms that are structure-sensitive, and which generally have lower activation energies, predominate over simple volume-diffusion at lower temperatures (Schmalzried 1974). Thus volume diffusion, which is kinetically favored and prevails at higher temperatures, tends to erase all evidence of growth zoning. At lower temperatures of metamorphism, and with increased Ag/Au and Ag/Hg activity ratios in the evolved pore-fluids, the diffusion-induced zoning is controlled by mechanisms that are structural-defect-dependent, such as surface diffusion and dislocation diffusion. Prior to reaching the temperature at which diffusion is effectively stopped, the kinetics of the diffusion mechanisms seem to have progressively impeded the attainment of equilibrium with falling temperature.

Conclusions

The Au–Ag–Hg alloy, the principal Au-bearing mineral identified at Trout Lake, is analogous to the *fcc* α-phase of the extrapolated Ag–Au–Hg system of Basu *et al.* (1981). Observed compositional range, inhomogeneity and zoning of the Trout Lake Au–Ag–Hg alloy confirm the existence of a field of extensive solid-solution corresponding to the α-phase. A general sequence of crystallization involving increasingly Ag-rich compositions suggests increased Ag/Au and Ag/Hg activity ratios with decreasing temperature of metamorphism, decreasing ΣS and increasing $f(O_2)$, together with disequilibrium conditions of crystallization. We conclude from textural and compositional evidence that the Au–Ag–Hg alloy crystallized from migrating pore-fluids, and not simply by exsolution from high-temperature pyrite. Approximately 7% of the Au in the ore is retained as "invisible" gold in arsenic-poor pyrite and arsenopyrite.

Gold is released from pyrite and exposed to pore fluids following pyrite metablastesis and subsequent fall in metamorphic temperatures, either by unmixing, as suggested by Boyle (1979), or by the total breakdown and replacement of pyrite in sheared ores. Primary coarse free grains of "gold" also would be susceptible to hydrothermal remobilization in the pore fluids. The Au is transported as bisulfide complexes and precipitated from the pore fluids at preferred sites by surface adsorption and reduction onto pyrite grains, or in conduits of high fluid-flow and low chemical potential in highly sheared Chalcopyrite Stringer ores. Thus, the crystallization of Au–Ag–Hg alloy can be considered a retrograde metamorphic process. The distribution of Au in Trout Lake probably largely reflects its original distribution due to exhalation and diagenesis, modified during metamorphism by limited solid-state diffusion, hydrothermal mobilization, local migration and precipitation.

The 450°C isothermal section used here is an elevated, though nonetheless reasonable model for the greenschist-facies metamorphic grade at Trout Lake. However, as the crystallization of Au–Ag–Hg alloy is considered to be a retrograde process, the phase relations in the Ag–Au–Hg system at and below 400°C might be more appropriate. In the absence of reconnaissance microprobe studies, it is probable that Au–Ag–Hg alloy has been misidentified as electrum in many deposits.

Acknowledgements

We thank Drs. A.C. Turnock, M. Raudsepp, F.C. Hawthorne, J.L. Jambor, L.J. Cabri and B. Nesbitt for fruitful discussions and critical reviews of early drafts of the manuscript. Dr. L.J. Cabri and J.H.G. Laflamme are thanked for helpful discussion pertaining to the microprobe analyses and mineral chemistry. Ron Chapman provided able assistance relating to the initial microprobe analyses on the MAC V and wavelength-dispersion traverses on the CAMECA SX-50 at the University of Manitoba. We are grateful to Hudson Bay Mining & Smelting for permission to publish the manuscript, and to members of the staff for their assistance. The manuscript was substantially improved through the critical review and many insightful comments of R.F. Martin and two anonymous referees. The study, which includes the cyanidation and SIMS analyses done under contract by S. L. Chryssoulis at the University of Western Ontario, was funded by a grant to Hudson Bay Mining & Smelting under the Canada–Manitoba Mineral Development Agreement.

References

Aggarwal, P. K. & Nesbitt, B. E. (1987): Pressure and temperature conditions of metamorphism in the vicinity of three massive sulfide deposits, Flin Flon — Snow Lake Belt, Manitoba. *Can. J. Earth Sci.* **24**, 2305-2315.

BANCROFT, G. M. & JEAN, G. (1982): Gold deposition at low temperature on sulphide minerals. *Nature* **298**, 730-731.

BARNES, H. L., ROMBERGER, S. B. & STEMPROK, M. (1967): Ore solution chemistry. II. Solubility of HgS in sulfide solutions. *Econ. Geol.* **62**, 957-982.

BASU, K., BORTNYKOV, N., MOOKHERJEE, A., MOZGOVA, N. & TSEPIN, A. I. (1981): Rare minerals from Rajpura-Dariba, Rajasthan, India. II. Intermetallic compound $Ag_{74.2}Au_{16.4}Hg_{9.4}$. *Neues Jahrb. Mineral., Abh.* **141**, 217-223.

BOYLE, R. W. (1979): The geochemistry of gold and its deposits. *Geol. Surv. Can. Bull.* **280.**

CABRI, L. J., CHRYSSOULIS, S. L., DE VILLIERS, J. P. R., LAFLAMME, J. H. G. & BUSECK, P. R. (1989): The nature of "invisible" gold in arsenopyrite. *Can. Mineral.* **27**, 353-362.

CATHLES, L. M. (1986): The geologic solubility of gold from 200-350°C, and its implications for gold - base metal ratios in vein and stratiform deposits. *In* Gold in the Western Shield (L. A. Clark, ed.). *Can. Inst. Min. Metall. Spec. Vol.* **38**, 187-210.

CHRYSSOULIS, S., CABRI, L. J. & SALTER, R. S. (1987): Direct determination of invisible gold in refractory sulphide ores (R. S. Salter, D. M. Wyslouzil & G. W. McDonald, eds.). *Proc. Int. Symp. on Gold Metallurgy, 1. Proc. Metall. Soc. of the Can. Inst. Min. Metall.*, 235-244.

COOK, N. J. & CHRYSSOULIS, S. L. (1989): Mineralogy of 'invisible' gold. *Geol. Assoc. Can. — Mineral. Assoc. Can., Program Abstr.* **14**, A134.

DUNN, P. J., CHAO, G. Y., FLEISCHER, M., FERRAIOLO, J. A., LANGLEY, R. H., PABST, A. & ZILCZER, J. A. (1985): New mineral names. *Am. Mineral.* **70**, 214-221.

ELDRIDGE, C. S., BARTON, P. B. & OHMOTO, H. (1983): Mineral textures and their bearing on the formation of the Kuroko orebodies. *In* The Kuroko and Related Volcanogenic Massive Sulphide Deposits (H. Ohmoto & B. J. Skinner, Jr., eds.). *Econ. Geol., Monogr.* **5**, 241-281.

FRANKLIN, J. M., LYDON, J. W. & SANGSTER, D. F. (1981): Volcanic-associated massive sulfide deposits. *Econ. Geol. 75th Anniv. Vol.*, 485-627.

GASPARRINI, C. (1983): The mineralogy of gold and its significance in metal extraction. *Can. Inst. Min. Metall. Bull.* **76**(851), 144-153.

HANNINGTON, M. D. & SCOTT, S. D. (1988): Gold and silver potential of polymetallic sulfide deposits on the sea floor. *Mar. Mining* **7**, 271-285.

HARRIS, D. C. (1986): Mineralogy and geochemistry of the main Hemlo gold deposit, Hemlo, Ontario, Canada. *In* Gold '86 (A. J. MacDonald, ed.). *Proc. Int. Symp. on Geology of Gold* (Toronto), 297-310.

HAUSEN, D. M. (1981): Process mineralogy of auriferous pyritic ores at Carlin, Nevada. *In* Process Mineralogy I (D. M. Hausen & W. C. Park, eds.). *Proc. SME-AIME Conf.* (New York), 271-289.

HEALY, R. E. & PETRUK, W. (1988): The mineral characteristics that affect metal recoveries from Cu, Zn, Pb and Ag ores in Manitoba. I. An investigation of the ore mineralogy of the Trout Lake deposit. *CANMET Invest. Rep.* **MSL 88-61**(IR).

_____ & _____ (1989): The mineral characteristics that affect metal recoveries from Cu, Zn, Pb and Ag ores in Manitoba. II. A mineralogical evaluation of the behaviour of metallic minerals in the Trout Lake concentrator circuit. *CANMET Invest. Rep.* **MSL 89-87**(IR).

HUSTON, D. L. & LARGE, R. R. (1989): A chemical model for the concentration of gold in volcanogenic massive sulphide deposits. *Ore Geol. Reviews* **4**, 171-200.

JEAN, G. E. & BANCROFT, G. M. (1985): An XPS and SEM study of gold deposition at low temperatures on sulphide mineral surfaces: concentration of gold by adsorption/reduction. *Geochim. Cosmochim. Acta* **49**, 979-987.

_____ & _____ (1986): Heavy metal adsorption by sulfide mineral surfaces. *Geochim. Cosmochim. Acta* **50**, 1455-1463.

KO, C. B. (1986): Geology of the Trout Lake copper-zinc sulphide deposit. *Hudson Bay Mining & Smelting, Internal Report.*

KOO, J. & MOSSMAN, D. J. (1975): Origin and metamorphism of the Flin Flon stratabound Cu-Zn sulphide deposit, Saskatchewan and Manitoba. *Econ. Geol.* **70**, 48-62.

LARGE, R. R. (1977): Chemical evolution and zonation of massive sulfide deposits in volcanic terrains. *Econ. Geol.* **72**, 549-572.

LOOMIS, T. P. (1983): Compositional zoning of crystals: a record of growth and reaction history. *In* Kinetics and Equilibrium in Mineral Reactions (S. K. Saxena, ed.). Springer Verlag, New York.

MCEACHERN, N. C. (1987): Trout Lake — recovery of Au & Ag from mill tailings. *Hudson Bay Mining & Smelting, Internal Report.*

MILOJKOVIC, D. (1983): Precious metal recovery from Flin Flon mill tailings. Progress Report #1. Cyanidation of Trout Lake zinc tailings. *Hudson Bay Mining & Smelting, Internal Report.*

MUZYLOWSKI, M. (1979): Copper-zinc discovery, Flin Flon, Manitoba. *Can. Mining J.* **100**(5), 65-67.

NAZMOVA, G. N. & SPIRIDONOV, E. M. (1979): Mercury-rich gold. *Dokl. Acad. Sci. SSSR, Earth Sci. Sect.* **246**, 138-141.

NYSTEN, P. (1986): Gold in the volcanogenic mercury-rich sulphide deposit Langsele, Skellefte ore district, northern Sweden. *Miner. Deposita* **21**, 116-120.

OBERTHUR, T. & SAAGER, R. (1986): Silver and mercury in gold particles from the Proterozoic Witwatersrand placer deposits of South Africa: metallogenic and geochemical implications. *Econ. Geol.* **81**, 20-31.

OZEROVA, N. A., PETSOVIC, M. S. & MURAVITSKAJA, G. N. (1980): Microcontents of mercury as a typomorphic characteristic of gold deposits. *In* Scientific Bases and Utilization of Typomorphism of Minerals (A. V. Siderenko, ed.). Nauka, Moscow.

PETRUK, W. (1987): Recent developments in process mineralogy of complex sulphide ores. *CANMET Rep. MSL* **87-1E.**

_____ (1988): Automatic image analysis for mineral beneficiation. *J. Metals* **40**(4), 29-31.

PINARD, R. G. & PETRUK, W. (1989): Silver content of galena from Trout Lake deposit in Flin Flon. *CANMET, Process Mineral. Sect. Rep.* **M-4070.**

PISUTHA-ARNOND, V. & OHMOTO, H. (1983): Thermal history, and chemical and isotopic compositions of the ore-forming fluids responsible for the Kuroko massive sulfide deposits in the Hokuroko district of Japan. *In* The Kuroko and Related Volcanogenic Massive Sulfide Deposits (H. Ohmoto & B. J. Skinner, Jr., eds.). *Econ. Geol., Monogr.* **5**, 523-558.

PUDDEPHATT, R.J. (1972): *The Periodic Table of the Elements.* Oxford University Press, Oxford, England.

ROMBERGER, S. B. (1986): The solution chemistry of gold applied to the origin of hydrothermal deposits. *In* Gold in the Western Shield (L. A. Clark, ed.). *Can. Inst. Min. Metall. Spec. Vol.* **7**, 168-186.

SCHMALZRIED, H. (1974): *Solid State Reactions.* Academic Press. New York.

SCOTT, J. D. (1977): Interim report on a mineralogical examination of ore specimens from the Centennial mine, Flin Flon, Manitoba. *Hudson Bay Mining & Smelting, Internal Report.*

SEWARD, T. M. (1984): The transport and deposition of gold in hydrothermal systems. *In* Gold'82: The Geology, Geochemistry and Genesis of Gold Deposits (R. P. Foster, ed.). *Geol. Soc. Zimbabwe Spec. Publ.* **1**, 165-181.

SHIKAZONO, N. & SHIMIZU, M. (1987): The Au/Ag ratio of native gold and electrum and the geochemical environment of gold vein deposits in Japan. *Miner. Deposita* **22**, 309-314.

_____ & _____ (1988): Mercurian gold from the Tsugu gold–antimony vein deposit in Japan. *Can. Mineral.* **26**, 423-428.

SPRINGER, J. S. (1983): Invisible gold. *In* The Geology of Gold in Ontario (A. C. Colvine, ed.). *Ont. Geol. Surv. Misc. Pap.* **110.**

_____ (1985): Carbon in Archean rocks of the Abitibi belt (Ontario–Quebec) and its relation to gold distribution. *Can. J. Earth Sci.* **22**, 1945-1951.

SUGAKI, A., SCOTT, S. D., HAYAHSI, K. & KITAKAZE, A. (1987): Ag_2S solubility in sulfide solutions up to 250°C. *Geochem. J.* **21**, 291-305.

SYME, E. C., BAILES, A. H., PRICE, D. P. & ZIEHLKE, D. V. (1982): Flin Flon volcanic belt: geology and ore deposits at Flin Flon and Snow Lake, Manitoba. *Geol. Assoc. Can. - Mineral. Assoc. Can., Field Trip Guidebook* **6.**

WELLS, J.D. & MULLENS, T. E. (1973): Gold-bearing arsenian pyrite determined by microprobe analysis, Cortez and Carlin gold mines, Nevada. *Econ. Geol.* **68**, 187-201.

WELLS, J. T. & GHORSO, M. S. (1988): Rock alteration, mercury transport, and metal deposition at Sulphur Bank, California. *Econ. Geol.* **83**, 606-618.

WILSON, G. C. & RUCKLIDGE, J. C. (1987): Mineralogy and microstructures of carbonaceous gold ores. *Mineral. Petrol.* **36**, 219-239.

Received November 22, 1988, revised manuscript accepted January 12, 1990.